Available online at www.sciencedirect.com
ScienceDirect
International Journal of Heat and Mass Transfer 51 (2008) 1379–1392
International Journal of HEAT and MASS TRANSFER
www.elsevier.com/locate/ijhmt

Free convection from elliptic cylinders at small Grashof numbers

S.J.D. D'Alessio [a,*], L.A. Finlay [a], J.P. Pascal [b]

[a] Department of Applied Mathematics, University of Waterloo, Waterloo, Ont., Canada N2L 3G1
[b] Department of Mathematics, Ryerson University, Toronto, Ont., Canada M5B 2K3

Received 14 March 2007; received in revised form 18 August 2007
Available online 31 December 2007

Abstract

This paper discusses and contrasts the steady and unsteady two-dimensional problem of laminar free convection from an inclined elliptic cylinder for small Grashof numbers. The governing Navier–Stokes and heat equations are formulated in terms of the streamfunction and vorticity. The results demonstrate that the steady and limiting unsteady flows are in good agreement near the cylinder surface while interesting departures occur in the far-field. Both numerical and analytical results are presented.

1. Introduction

Natural, or free, convection from a horizontal two-dimensional body is a fundamental thermal-fluid problem. It has received numerous numerical, experimental and theoretical studies over the years. This paper deals with the steady and unsteady problem of laminar, two-dimensional flow caused by free convection from an isothermal inclined elliptic cylinder in a fluid which is initially at rest. The main assumptions made in this study are that the flow remains laminar and two-dimensional for all time, $t > 0$. Simplifications made include the Boussinesq approximation and the neglect of viscous dissipation. For the small Grashof number range considered here, these simplifications are quite reasonable.

This problem is of interest for both theoretical and practical reasons since it has important applications in engineering such as flow past heated tubes or wires, hot wire anemometry, thermal pollution, dispersion of pollutants, and even in the design of heat exchangers. The related problems of the heated flat plate and the heated circular cylinder are well studied and some of these works include [1–15].

Relatively little work has been done for the more general geometry of an elliptic cylinder which is considered here. The main motivation for pursuing the elliptic geometry lies in the enhancement in the rate of heat transfer associated with this. It is thus important to quantify this enhancement. An added advantage offered is that the elliptic geometry is flexible enough to tackle all elliptic cross sections ranging from the limiting case of a circular cylinder to that of a flat plate. Some existing research includes the studies of Badr and Shamsher [16] and Mahfouz and Kocabiyik [17] who address the symmetrical unsteady case and the study of Badr [18] which considers asymmetrical flows. Some important experimental investigations were carried out by Huang and Mayinger [19] for elliptic tubes at various inclinations and aspect ratios and more recently by Elsayed et al. [20] for the case of a constant heat flux from an elliptic tube at large Grashof numbers.

The present work differs from previous studies in a few respects. First, we are interested in both the steady and unsteady cases and have carried out a detailed investigation into the similarities and differences between these problems for the small Grashof number regime. Specifically, we investigate whether the unsteady problem converges to the steady-state problem for large times. Further, this work offers analytical results for both the steady and unsteady problems. For the steady-state case an asymptotic solution valid at large distances is derived and used to furnish

* Corresponding author. Tel.: +1 519 888 4567x35014; fax: +1 519 746 0274.
E-mail address: sdalessio@uwaterloo.ca (S.J.D. D'Alessio).

0017-9310/$ - see front matter © 2007 Elsevier Ltd. All rights reserved.
doi:10.1016/j.ijheatmasstransfer.2007.11.020

Nomenclature

a_1, a_2	arbitrary constants in asymptotic solution
b, a	cylinder semi-minor, semi-major axes, respectively
c_0, c_1, c_2, c_3, c_4	finite differencing constants
A, B, A_0, B_0, A_1, B_1	functions appearing in governing equations
c	semi-focal length, $c = \sqrt{a^2 - b^2}$
g	gravitational acceleration
Gr	Grashof number, $Gr = \alpha g c^3 (T_0 - T_\infty)/\nu^2$
h, k	uniform grid spacing in ξ, θ directions, respectively
H	computational parameter, $H = h/k$
K	number of terms retained in Fourier series
M	metric of transformation
M_0	metric evaluated on the cylinder surface
Nu	local Nusselt number
$N \times L$	computational grid
$\overline{Nu}$	average Nusselt number
Pr	Prandtl number, $Pr = \nu/\kappa$
q, Q	functions representing right-hand-sides
r	ellipse aspect ratio, $r = b/a$
r_n, s_n	Fourier coefficients for the vorticity
S_1, S_2, S_3	source terms
t	time
T	dimensional temperature
v_ξ, v_θ	velocity components
x, y	Cartesian coordinates
z	boundary-layer coordinate
z_∞	outer boundary

Greek symbols

α	thermal expansion coefficient
β	computational parameter
Δt	time increment in numerical scheme
ε	tolerance
κ	thermal diffusivity
ν	kinematic viscosity
ξ, θ	elliptic coordinates
ξ_0	constant related to r, $\tanh \xi_0 = r$
ξ_∞	outer boundary
η	angle of inclination
λ	boundary-layer parameter, $\lambda = \sqrt{4t}$
ϕ	dimensionless temperature, $\phi = (T - T_\infty)/(T_0 - T_\infty)$
Φ	scaled dimensionless temperature, $\Phi(\xi, \theta) = \phi(\xi, \theta) - e^{-4\xi}$
ψ	streamfunction
ζ	vorticity
χ	generic flow variable

Subscripts

0	surface value or leading-order terms
∞	value at infinity

Superscript

$\sim$	dimensional quantity

far-field boundary conditions for the steady numerical solution procedure. Previous asymptotic solutions, some of which include the works [21–25], revolve around the simplified boundary-layer equations which are appropriate near the cylinder and for large Grashof numbers. These solutions are not expected to be valid in the buoyant plume region, especially for small Grashof numbers. The asymptotic solution presented in our research is not based on the boundary-layer equations and thus applies in the far-field. For the unsteady case an approximate analytical solution valid for small times is constructed and used to provide an initial condition for the unsteady numerical solution procedure.

The paper is organized as follows. In the following section we present the governing equations which are formulated in terms of the streamfunction and vorticity and introduce a coordinate system which is convenient for the elliptic geometry. Then, in Section 3 we discuss numerical techniques used to solve the steady and unsteady problems. In describing the numerical schemes, the difficulties associated with solving the steady and unsteady equations will be pointed out and ways of overcoming these inherent difficulties will be proposed. Following this, in Section 4, we present and discuss the numerical results obtained. A brief summary outlining the key points is included in the concluding section. Lastly, Appendices A and B outline the asymptotic and small time analyses, respectively.

2. Governing equations

The equations governing the motion of a viscous incompressible fluid are the Navier–Stokes and energy equations. The fluid is characterized by the following properties: ν the kinematic viscosity, κ the thermal diffusivity, α the thermal expansion coefficient, and k the thermal conductivity. While these fluid properties are assumed to be constant, the fluid density, ρ, is allowed to vary with temperature, T, in the usual fashion

$$\rho(T) = \rho_0[1 - \alpha(T - T_\infty)],$$

where ρ_0 refers to a reference density and T_∞ the constant far-field temperature. To render the equations in dimensionless form the chosen length scale is the semi-focal length of the ellipse, $c = \sqrt{a^2 - b^2}$ (where a, b denote the semi-major and semi-minor axis lengths, respectively), the

time scale is c^2/ν and the temperature scale is $T_0 - T_\infty$ where T_0 is the constant surface temperature.

Since the flow is assumed to remain two-dimensional it is beneficial to work in terms of a streamfunction and vorticity. Also, because of the geometry of the problem it is worthwhile to work with the modified polar coordinates (ξ, θ) which are related to the Cartesian coordinates (x, y) through the conformal transformation

$$x + \mathrm{i}y = \cosh[(\xi + \xi_0) + \mathrm{i}\theta].$$

The advantage of this is that the contour of the cylinder is transformed to $\xi = 0$ while the infinite region exterior to the cylinder is mapped to the semi-infinite rectangular strip $0 < \xi < \infty$, $-\pi \leqslant \theta \leqslant \pi$. The constant ξ_0 is defined by

$$\tanh \xi_0 = r,$$

where $r = b/a$ is the ellipse aspect ratio. The above mapping holds for all elliptic cylinders having $0 < r < 1$ with $r = 0$ denoting a flat plate and $r = 1$ a circular cylinder. Another important feature associated with this transformation is that length scales close to the cylinder remain unchanged while those far away get contracted. This is helpful from a numerical point of view since the flow field is compressed.

The flow configuration is illustrated in Fig. 1. We now proceed to write the steady and unsteady equations of motion.

2.1. Steady-state problem

In terms of the coordinates (ξ, θ) the dimensionless steady-state Navier–Stokes and energy equations for a viscous, incompressible fluid in terms of the streamfunction, ψ, vorticity, ζ, and temperature, ϕ, then become

$$\frac{\partial^2\psi}{\partial\xi^2} + \frac{\partial^2\psi}{\partial\theta^2} = M^2\zeta, \tag{1}$$

$$\frac{\partial^2\zeta}{\partial\xi^2} + \frac{\partial^2\zeta}{\partial\theta^2} = \frac{\partial\psi}{\partial\xi}\frac{\partial\zeta}{\partial\theta} - \frac{\partial\psi}{\partial\theta}\frac{\partial\zeta}{\partial\xi} - Gr\left(A\frac{\partial\phi}{\partial\xi} - B\frac{\partial\phi}{\partial\theta}\right), \tag{2}$$

$$\frac{\partial^2\phi}{\partial\xi^2} + \frac{\partial^2\phi}{\partial\theta^2} = Pr\left(\frac{\partial\psi}{\partial\xi}\frac{\partial\phi}{\partial\theta} - \frac{\partial\psi}{\partial\theta}\frac{\partial\phi}{\partial\xi}\right), \tag{3}$$

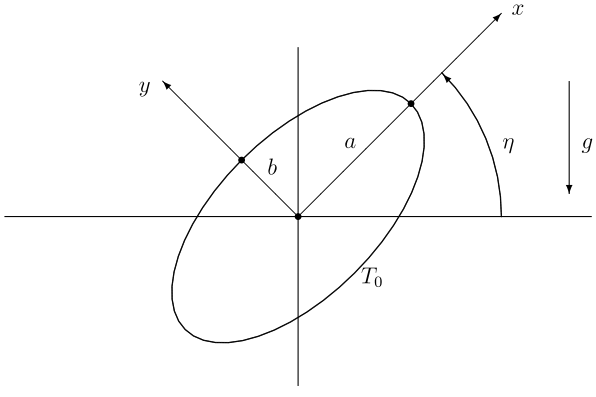

Fig. 1. The flow configuration.

where

$$M^2 = \frac{1}{2}[\cosh(2(\xi + \xi_0)) - \cos(2\theta)],$$

$$A = \sinh(\xi + \xi_0)\cos(\eta)\cos(\theta) - \cosh(\xi + \xi_0)\sin(\eta)\sin(\theta),$$

$$B = \cosh(\xi + \xi_0)\cos(\eta)\sin(\theta) + \sinh(\xi + \xi_0)\sin(\eta)\cos(\theta).$$

The velocity components (v_ξ, v_θ) in the directions of increase of (ξ, θ) are related to the streamfunction through

$$v_\xi = -\frac{1}{M}\frac{\partial\psi}{\partial\theta}, \quad v_\theta = \frac{1}{M}\frac{\partial\psi}{\partial\xi},$$

while the vorticity is found through the expression

$$\zeta = \frac{1}{M^2}\left(\frac{\partial}{\partial\xi}(Mv_\theta) - \frac{\partial}{\partial\theta}(Mv_\xi)\right).$$

The problem as posed is completely specified by the following dimensionless parameters: the Grashof number, $Gr = \alpha g c^3(T_0 - T_\infty)/\nu^2$, the inclination, η, the Prandtl number, $Pr = \nu/\kappa$, and the ellipse parameter, r. The dimensionless temperature, ϕ, is related to the dimensional temperature, T, through $\phi = (T - T_\infty)/(T_0 - T_\infty)$. Similarly, $\psi = \tilde{\psi}/\nu$ and $\zeta = c^2\tilde{\zeta}/\nu$ with the tilde denoting a dimensional quantity. Lastly, in arriving at the above equations we have made the Boussinesq approximation to describe the buoyancy force and have omitted viscous dissipation.

Eqs. (1)–(3) are to be solved subject to the no-slip and isothermal boundary conditions on the surface given by

$$\psi = \frac{\partial\psi}{\partial\xi} = 0 \quad \text{and} \quad \phi = 1 \ \text{ on } \ \xi = 0.$$

Inspecting these conditions we observe that two conditions for the streamfunction are given while none are provided for the vorticity. Later we will discuss a method to prescribe the surface vorticity. The vorticity field can be shown [26] to satisfy integral constraints. These can be derived from the boundary conditions using Green's second identity and are given by

$$\int_0^\infty \int_{-\pi}^{\pi} \mathrm{e}^{-n\xi} M^2\zeta \sin(n\theta)\mathrm{d}\theta\mathrm{d}\xi = 0, \quad n = 1, 2, \ldots,$$

$$\int_0^\infty \int_{-\pi}^{\pi} \mathrm{e}^{-n\xi} M^2\zeta \cos(n\theta)\mathrm{d}\theta\mathrm{d}\xi = 0, \quad n = 0, 1, \ldots$$

While the far-field conditions are simply

$$\psi, \zeta, \phi \to 0 \quad \text{as } \ \xi \to \infty,$$

we have carried out an asymptotic analysis, presented in Appendix A, and have derived more appropriate far-field gradient conditions given by

$$\frac{\partial\psi}{\partial\xi} \to -\psi, \quad \frac{\partial\zeta}{\partial\xi} \to -3\zeta, \quad \frac{\partial\phi}{\partial\xi} \to -4\phi \ \text{ as } \ \xi \to \infty.$$

These conditions have the effect of bringing infinity closer and enables a smaller computational grid to be used. Lastly, periodicity is enforced in all the flow variables.

2.2. Unsteady problem

For the unsteady problem we assume that at $t = 0$ the temperature of the cylinder surface is set to T_0 while the surrounding fluid temperature is T_∞ with $T_0 > T_\infty$. Impulsively generated convection will then form as a result of the discontinuity in temperature. The unsteady problem is governed by the streamfunction equation (1) together with the following dimensionless vorticity and heat transport equations:

$$\frac{\partial\zeta}{\partial t} = \frac{1}{M^2}\left[-\frac{\partial\psi}{\partial\xi}\frac{\partial\zeta}{\partial\theta} + \frac{\partial\psi}{\partial\theta}\frac{\partial\zeta}{\partial\xi} + \frac{\partial^2\zeta}{\partial\xi^2} + \frac{\partial^2\zeta}{\partial\theta^2} + Gr\left(A\frac{\partial\phi}{\partial\xi} - B\frac{\partial\phi}{\partial\theta}\right)\right], \tag{4}$$

$$\frac{\partial\phi}{\partial t} = \frac{1}{M^2}\left[-\frac{\partial\psi}{\partial\xi}\frac{\partial\phi}{\partial\theta} + \frac{\partial\psi}{\partial\theta}\frac{\partial\phi}{\partial\xi} + \frac{1}{Pr}\left(\frac{\partial^2\phi}{\partial\xi^2} + \frac{\partial^2\phi}{\partial\theta^2}\right)\right]. \tag{5}$$

Boundary conditions valid for all $t \geqslant 0$ for the unsteady problem include the no-slip and isothermal surface conditions, and the periodicity and integral conditions presented earlier, along with

$$\psi, \zeta, \phi \to 0 \quad \text{as} \quad \xi \to \infty,$$

which correspond to a quiescent ambient far-field flow. We note that these conditions are appropriate for solving the time-dependent problem because in this case heat and momentum require some time to diffuse away from the cylinder surface and we can always place the outer boundary sufficiently far away to guarantee this. In the steady-state, or time-independent, case this is not possible. Lastly, we need to specify initial conditions. Since the fluid motion starts from rest, the initial conditions for ψ and ζ are simply

$$\psi(\xi, \theta, t = 0) = \zeta(\xi, \theta, t = 0) = 0.$$

The initial temperature distribution, on the other hand, will be given by

$$\phi(\xi, \theta, t = 0) = \begin{cases} 1 & \text{on } \xi = 0 \\ 0 & \text{for } \xi \neq 0 \end{cases}.$$

As previously mentioned, the discontinuity in the initial temperature field gives rise to an infinite heat flux bleeding off the cylinder surface at $t = 0$. To partially account for this inherent singularity we make the following boundary-layer type transformation:

$$\xi = \lambda z, \quad \lambda = \sqrt{4t}. \tag{6}$$

The similarity variable z is actually suggested by the approximate solution derived in Appendix B for small times t. Essentially, this change of variable stretches the initial thin thermal-boundary layer. A similar transformation has been successfully used in the recent investigation by D'Alessio et al. [27] involving mixed and forced convection. The analysis presented in Appendix B demonstrates that this approach can also be applied to free convection problems.

In terms of the coordinate z Eqs. (1), (4), and (5) now become

$$\frac{\partial^2\psi}{\partial z^2} + 4t\frac{\partial^2\psi}{\partial\theta^2} = 4tM^2\zeta, \tag{7}$$

$$\frac{1}{M^2}\frac{\partial^2\zeta}{\partial z^2} + 2z\frac{\partial\zeta}{\partial z} = 4t\frac{\partial\zeta}{\partial t} - \frac{4t}{M^2}\frac{\partial^2\zeta}{\partial\theta^2} - \frac{2\sqrt{t}}{M^2}\left(\frac{\partial\psi}{\partial\theta}\frac{\partial\zeta}{\partial z} - \frac{\partial\psi}{\partial z}\frac{\partial\zeta}{\partial\theta}\right) - \frac{2Gr\sqrt{t}}{M^2}\left(A\frac{\partial\phi}{\partial z} - 2B\sqrt{t}\frac{\partial\phi}{\partial\theta}\right), \tag{8}$$

$$\frac{1}{PrM^2}\frac{\partial^2\phi}{\partial z^2} + 2z\frac{\partial\phi}{\partial z} = 4t\frac{\partial\phi}{\partial t} - \frac{4t}{PrM^2}\frac{\partial^2\phi}{\partial\theta^2} - \frac{2\sqrt{t}}{M^2}\left(\frac{\partial\psi}{\partial\theta}\frac{\partial\phi}{\partial z} - \frac{\partial\psi}{\partial z}\frac{\partial\phi}{\partial\theta}\right), \tag{9}$$

and will be used to dictate the early stages of the flow. Once the boundary layer thickens appreciably it is unrealistic to continue working in terms of the boundary-layer coordinate z. We then switch back to the original coordinate ξ and solve Eqs. (1), (4), and (5). To avoid the temperature discontinuity at $t = 0$ an approximate solution was used as an initial condition at a small time beyond $t = 0$. The approximate solution, derived in Appendix B, is valid for small times and is implemented at a time when it is judged to be valid. As a final note we emphasize that although the boundary-layer coordinate z is utilized, the fully nonlinear Navier–Stokes and energy equations are to be solved and not the simplified boundary-layer equations.

3. Numerical methods

We begin by discretizing the computational domain bounded by $0 \leqslant \xi \leqslant \xi_\infty$ and $-\pi \leqslant \theta \leqslant \pi$ into a uniform network of $N \times L$ grid points located at

$$\xi_i = ih, \quad i = 0, 1, \ldots, N,$$
$$\theta_j = -\pi + jk, \quad j = 0, 1, \ldots, L$$

with

$$h = \frac{\xi_\infty}{N},$$
$$k = \frac{2\pi}{L},$$

where ξ_∞ denotes the outer boundary approximating infinity.

3.1. Steady-state calculations

The steady-state equations (1)–(3) are solved by finite differences. Defining $\chi_{i,j} \equiv \chi(\xi_i, \theta_j)$ where χ denotes a generic flow variable, we can obtain discretized versions of Eqs. (1)–(3). Using central differencing the discretized version of the streamfunction equation (1) becomes

$$2(1 + H^2)\psi_{i,j} = \psi_{i+1,j} + \psi_{i-1,j} + H^2(\psi_{i,j+1} + \psi_{i,j-1}) - h^2M^2_{i,j}\zeta_{i,j},$$

where $H = h/k$. Prompted by the asymptotic analysis in Appendix A and the boundary conditions satisfied by ϕ, we set $\phi = e^{-4\xi} + \Phi$. Then Eqs. (2) and (3) transform to

$$\frac{\partial^2\zeta}{\partial\xi^2}+\frac{\partial^2\zeta}{\partial\theta^2}=\frac{\partial\psi}{\partial\xi}\frac{\partial\zeta}{\partial\theta}-\frac{\partial\psi}{\partial\theta}\frac{\partial\zeta}{\partial\xi} - Gr\left(A\left(-4e^{-4\xi}+\frac{\partial\Phi}{\partial\xi}\right)-B\frac{\partial\Phi}{\partial\theta}\right), \tag{10}$$

$$\frac{\partial^2\Phi}{\partial\xi^2}+\frac{\partial^2\Phi}{\partial\theta^2}=-16e^{-4\xi}+Pr\left(\frac{\partial\psi}{\partial\xi}\frac{\partial\Phi}{\partial\theta}-\frac{\partial\psi}{\partial\theta}\left(-4e^{-4\xi}+\frac{\partial\Phi}{\partial\xi}\right)\right), \tag{11}$$

and Φ satisfies simpler boundary conditions given by

$$\Phi=0 \quad \text{on} \quad \xi=0, \quad \frac{\partial\Phi}{\partial\xi}\to-4\Phi \quad \text{as} \quad \xi\to\infty. \tag{12}$$

Since Eqs. (10) and (11) are similar in form we rewrite them in the generic form

$$\frac{\partial^2\chi}{\partial\xi^2}+\frac{\partial^2\chi}{\partial\theta^2}=a_4\left(\frac{\partial\psi}{\partial\xi}\frac{\partial\chi}{\partial\theta}-\frac{\partial\psi}{\partial\theta}\frac{\partial\chi}{\partial\xi}\right)+S_1.$$

To solve the above we apply a generalized second-order discretization scheme given by

$$c_0\chi_{i,j}=c_1\chi_{i+1,j}+c_2\chi_{i-1,j}+c_3\chi_{i,j+1}+c_4\chi_{i,j-1}-h^2S_1,$$

where

$$c_0=2+2H^2+2\beta\left(\frac{a_4H}{4}\right)^2[(\Delta\psi_\theta)^2+(\Delta\psi_\xi)^2],$$

$$c_1=1+\frac{a_4H}{4}\Delta\psi_\theta+\beta\left(\frac{a_4H}{4}\right)^2(\Delta\psi_\theta)^2,$$

$$c_2=1-\frac{a_4H}{4}\Delta\psi_\theta+\beta\left(\frac{a_4H}{4}\right)^2(\Delta\psi_\theta)^2,$$

$$c_3=H^2-\frac{a_4H}{4}\Delta\psi_\xi+\beta\left(\frac{a_4H}{4}\right)^2(\Delta\psi_\xi)^2,$$

$$c_4=H^2+\frac{a_4H}{4}\Delta\psi_\xi+\beta\left(\frac{a_4H}{4}\right)^2(\Delta\psi_\xi)^2,$$

with

$$\Delta\psi_\xi=\psi_{i+1,j}-\psi_{i-1,j}, \quad \Delta\psi_\theta=\psi_{i,j+1}-\psi_{i,j-1}.$$

In the above scheme β is a computational parameter yet to be defined. Clearly, when $\beta=0$ the scheme reduces to the usual central-difference representation. Further, if $\beta\geqslant 1/4$ then the associated matrix is diagonally dominant and therefore an iterative method of solution should converge. It is interesting to point out that with the choice of $\beta=1/3$ all the terms present in the above appear as part of the compact h^4-accurate schemes of Dennis and Hudson [28].

As previously mentioned there is no condition for the surface vorticity. To circumvent this problem a second-order expression for the surface vorticity can be derived by taking a Taylor expansion of ψ about the cylinder surface and making use of the extra condition available for the streamfunction. This leads to the following formula for computing the surface vorticity, $\zeta_{o,j}$:

$$(3M_{o,j}^2+2h\sinh 2\xi_o)\zeta_{o,j}=\frac{12\psi_{1,j}}{h^2}-M_{o,j}^2(4\zeta_{1,j}-\zeta_{2,j})+O(h^2).$$

A computationally efficient way to enforce the far-field gradient conditions is through

$$\psi_{N,j}=e^{-h}\psi_{N-1,j},$$
$$\zeta_{N,j}=e^{-3h}\zeta_{N-1,j},$$
$$\Phi_{N,j}=e^{-4h}\Phi_{N-1,j}.$$

An iteration of the procedure involves sweeping through all the grid points using the above formulae to obtain a new approximation to ψ and χ and is repeated until the maximum value of the absolute difference between successive iterates falls below a specified tolerance ε.

3.2. Unsteady calculations

As previously mentioned the early stages of the flow are to be computed using Eqs. (7)–(9) involving the boundary-layer coordinate z. We point out that the physical coordinate $\xi=\lambda z$ is a moving coordinate and hence the outer boundary $\xi_\infty=\lambda z_\infty$ is constantly being pushed further away from the cylinder surface at a rate which reflects the initial growth of the thermal-boundary layer. For this reason we are justified in saying that no heat or vorticity will reach the outer boundary ξ_∞. Once the boundary layer thickens we change back to the coordinate ξ and solve (1), (4), (5). A convenient time to make the switch is at $t=0.25$ since at this time $\lambda=1$ and hence $\xi=z$.

The streamfunction equations (1) and (7) are solved by using standard central differencing as discussed in the previous section. To discuss the numerical method used to solve Eqs. (8) and (9) we begin by rewriting them in the generic form

$$t\frac{\partial\chi}{\partial t}=q(z,\theta,t),$$

where

$$q(z,\theta,t)=\frac{a_5}{4M^2}\frac{\partial^2\chi}{\partial z^2}+\frac{z}{2}\frac{\partial\chi}{\partial z}+\frac{a_5t}{M^2}\frac{\partial^2\chi}{\partial\theta^2} +\frac{2\sqrt{t}}{M^2}\left(\frac{\partial\psi}{\partial\theta}\frac{\partial\chi}{\partial z}-\frac{\partial\psi}{\partial z}\frac{\partial\chi}{\partial\theta}\right)+S_2.$$

The scheme used to discretize this equation is very similar to the Crank–Nicholson implicit procedure. Assuming the solution at time t is known, we advance the solution to time $t+\Delta t$ by integrating the above. Integration by parts yields

$$\chi\tau\big|_t^{t+\Delta t}-\int_t^{t+\Delta t}\chi\,d\tau=\int_t^{t+\Delta t}q\,d\tau,$$

where Δt is the time increment. Approximating the integrals using the trapezoidal rule results in the expression

$$\chi(z,\theta,t+\Delta t)=\chi(z,\theta,t)+\left(\frac{\Delta t}{2t+\Delta t}\right)[q(z,\theta,t+\Delta t)+q(z,\theta,t)].$$

Since $q(z,\theta,t+\Delta t)$ depends on $\chi(z,\theta,t+\Delta t)$ and its spacial derivatives the scheme is implicit. This equation is solved

iteratively using a Gauss–Seidel procedure with the spatial derivatives appearing in the function q being approximated by central-differences.

The boundary conditions used in solving the heat transport equation are straight-forward and require no explanation. For the vorticity transport equation, on the other hand, careful attention must be given in determining the surface vorticity. We begin by introducing the functions $r_n(z,t)$ and $s_n(z,t)$ defined by

$$r_n(z,t) = \frac{1}{\pi}\int_{-\pi}^{\pi} M^2\zeta \sin(n\theta)\mathrm{d}\theta; \quad n = 1,2,\ldots,$$
$$s_n(z,t) = \frac{1}{\pi}\int_{-\pi}^{\pi} M^2\zeta \cos(n\theta)\mathrm{d}\theta; \quad n = 0,1,\ldots$$

Referring back to the integral conditions, it is easy to see that these functions will satisfy the integral constraints given by

$$\int_0^{\infty} \mathrm{e}^{-n\lambda z} r_n(z,t)\mathrm{d}z = 0, \quad n = 1,2,\ldots,$$
$$\int_0^{\infty} \mathrm{e}^{-n\lambda z} s_n(z,t)\mathrm{d}z = 0, \quad n = 0,1,\ldots$$

The surface vorticity can be determined by inverting the expressions for r_n and s_n and leads to the truncated Fourier series

$$\zeta(0,\theta,t) = \frac{1}{M_0^2}\left\{\frac{1}{2}s_0(0,t) + \sum_{n=1}^{K}[r_n(0,t)\sin(n\theta) + s_n(0,t)\cos(n\theta)]\right\}.$$

The quantities $s_n(0,t)$ and $r_n(0,t)$ are computed by enforcing the integral conditions; that is, off the cylinder surface r_n and s_n can be computed using the most recent guess for ζ. Then, $s_n(0,t)$ and $r_n(0,t)$ are computed by numerically satisfying the integral constraints.

As previously mentioned, the temperature discontinuity at $t = 0$ is avoided by using an approximate solution, outlined in Appendix B, as an initial condition at a small time beyond $t = 0$. For $t > 0.25$ Eqs. (1), (4), and (5) are then solved. The numerical method used on Eqs. (4) and (5) is similar to that already described. The only difference worth pointing out is that for $t > 0.25$ these equations can be rewritten in the generic form

$$\frac{\partial\chi}{\partial t} = Q(\xi,\theta,t),$$

where

$$Q(\xi,\theta,t) = \frac{1}{M^2}\left[\frac{\partial\psi}{\partial\theta}\frac{\partial\chi}{\partial\xi} - \frac{\partial\psi}{\partial\xi}\frac{\partial\chi}{\partial\theta} + a_5\left(\frac{\partial^2\chi}{\partial\xi^2} + \frac{\partial^2\chi}{\partial\theta^2}\right) + S_3\right].$$

Using the same approach as previously outlined we arrive at the following scheme for solving the above transport equation:

$$\chi(\xi,\theta,t+\Delta t) = \chi(\xi,\theta,t) + \frac{\Delta t}{2}[Q(\xi,\theta,t+\Delta t) + Q(\xi,\theta,t)].$$

4. Numerical results and discussion

Here we present numerical results obtained by the methods discussed in the previous section. The problem of free convection from an inclined elliptic cylinder is completely characterized by the parameters Gr, Pr, η and r. Detailed numerical solutions have been obtained for small Grashof numbers in the range $1 \leqslant Gr \leqslant 20$ for inclinations 0°, 45°, 90°. Solutions were obtained for ellipses having $r = 0.2, 0.5, 0.8$ and for $Pr = 0.7, 1, 5, 10$.

4.1. Steady-state results

In obtaining steady-state solutions the symmetric problem corresponding to $\eta = 0°$ for a given Gr, Pr and r was first solved. This was then used as an initial guess for the asymmetric case with $\eta = 45°$. This was done in order to accelerate the convergence of the numerical procedure. As is usual with these types of problems, mild under-relaxation had to be applied in computing the surface vorticity.

In all our computations the parameter β was set to $\beta = 1/2$. With $\beta = 0$ (i.e., central differencing) convergence problems were encountered. The optimal values of the outer boundary location ξ_∞ and grid size $N \times L$ were determined by carrying out numerous numerical experiments. Two grid sizes (81×81 and 121×121) along with three choices of ξ_∞ (3, 4 and 5) were used. The values $\xi_\infty = 3, 4, 5$ correspond to locations of about 20, 50, 130 semi-major axis lengths, respectively. Listed in Table 1 are the resulting average Nusselt numbers ($\overline{Nu}$), defined as

$$\overline{Nu} = \frac{1}{2\pi}\int_{-\pi}^{\pi} Nu\mathrm{d}\theta \quad \text{where } Nu = -2\left(\frac{1}{M}\frac{\partial\phi}{\partial\xi}\right)_0,$$

for the various ξ_∞ and $N \times L$ values. The observed trend is that as ξ_∞ increases for a fixed grid size, $\overline{Nu}$ also increases. On the other hand, for a fixed ξ_∞, $\overline{Nu}$ decreases as the grid size increases. Since little change in $\overline{Nu}$ occurs when going from $\xi_\infty = 4$ to $\xi_\infty = 5$ for the grid size $N \times L = 121 \times 121$, these choices were adopted for all steady-state calculations and were found to be adequate for the Grashof and

Table 1
Comparison of $\overline{Nu}$ with different grids and outer boundary locations ξ_∞ for the case with $Pr = 0.7$, $Gr = 1$, $\eta = 45°$ and $r = 0.5$ using the gradient far-field condition

ξ_∞	Grid size	$\overline{Nu}$
3	81×81	1.443
4	81×81	1.525
5	81×81	1.604
3	121×121	1.391
4	121×121	1.452
5	121×121	1.484

Prandtl numbers considered. Convergence was defined when two successive iterates of the temperature, vorticity, streamfunction and Nusselt number differed by a tolerance of ϵ. Typically, $\epsilon \sim 10^{-6}$ was used.

In all isotherm plots to be presented, contours of $\phi = 0.1, \ldots, 1$ in increments of $\Delta\phi = 0.1$ are plotted. The outermost contour corresponds to $\phi = 0.1$ while the innermost contour corresponds to $\phi = 1$ which coincides with the cylinder surface. We observed a visible improvement in using the gradient far-field condition over the zero far-field condition. While the isotherms near the cylinder surface were found to be in close agreement, further away noticeable differences appeared: the solution using the zero far-field conditions exhibited mushrooming isotherms as a result of compressing the flow field whereas the gradient far-field conditions produced plume-like isotherms which are physically more realistic. This difference was most noticeable when $\xi_\infty = 3$. In addition, differences in the computed $\overline{Nu}$ resulted. For example, with $Pr = 0.7$, $Gr = 1$, $\eta = 45^\circ$, $r = 0.5$ (using $\xi_\infty = 5$ and $N \times L = 121 \times 121$) we obtained

$\overline{Nu} = 1.484$ using the gradient far-field condition, while

$\overline{Nu} = 1.555$ using the zero far-field condition.

Thus, unless otherwise specified, the gradient condition was used in obtaining all subsequent results. A streamline plot is shown in Fig. 2 corresponding to the case $Gr = 1, Pr = 1$, $r = 0.5$, $\eta = 45^\circ$; clearly visible in this diagram is the rising fluid motion above the cylinder and the recirculating flow on either side further aloft.

Figs. 3 and 4 illustrate the surface vorticity and Nusselt number distributions, respectively, for $Gr = 1, 10, 20$. Both plots reveal pronounced variations occurring near the tips of the cylinder as Gr is increased. Listed in Tables 2–4 are steady-state results for various parameter values. The dependence of $\overline{Nu}$ on the parameters is apparent. For a fixed r and η, $\overline{Nu}$ increases as either Gr or Pr increases, while $\overline{Nu}$ decreases as r is increased for a fixed Gr, Pr and

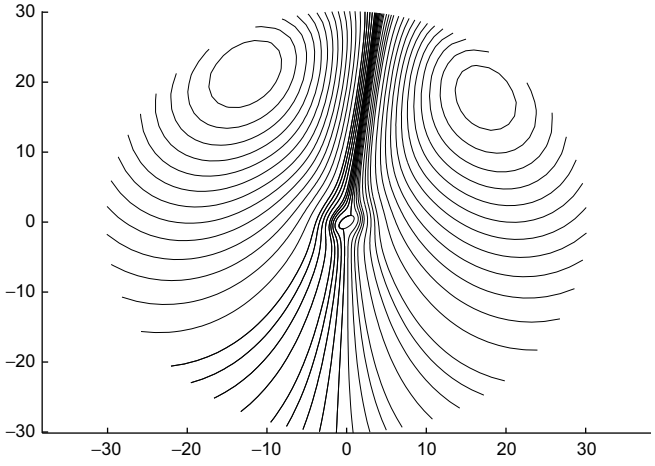

Fig. 2. Steady streamline plot for the case $Gr = 1, Pr = 1, r = 0.5, \eta = 45^\circ$.

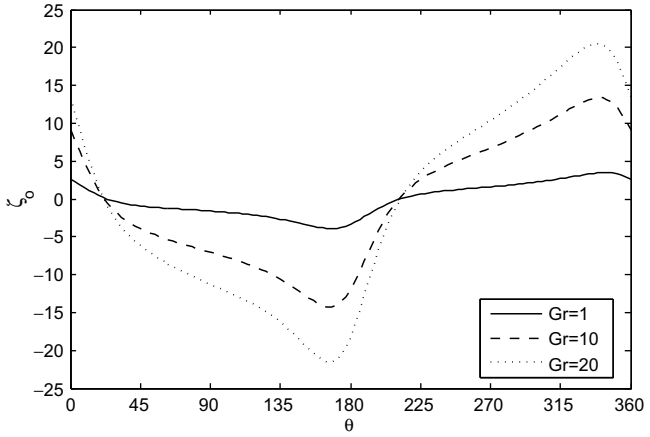

Fig. 3. Steady surface vorticity distributions for various Grashof numbers with $Pr = 1, r = 0.5, \eta = 45^\circ$.

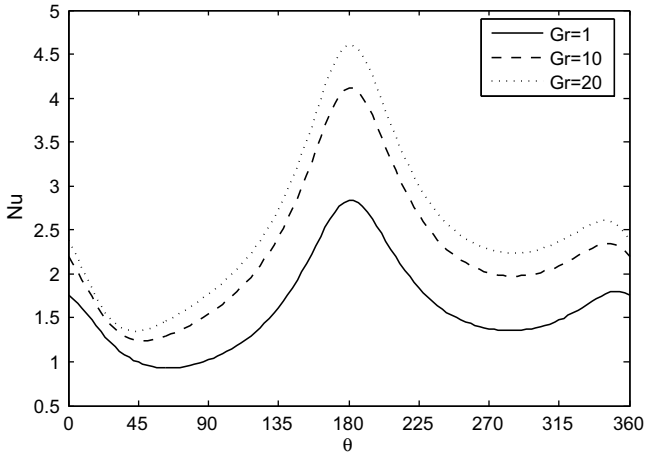

Fig. 4. Steady Nu distributions for various Grashof numbers with $Pr = 1, r = 0.5, \eta = 45^\circ$.

Table 2
Average Nusselt numbers for various Grashof numbers and inclinations with $Pr = 1$ and $r = 0.5$

η	$\overline{Nu}$		
	$Gr = 1$	$Gr = 10$	$Gr = 20$
0°	1.579	2.226	2.489
45°	1.603	2.272	2.545
90°	1.625	2.330	2.600

Table 3
Average Nusselt numbers for various Grashof numbers and aspect ratios with $Pr = 1$ and $\eta = 45^\circ$

r	$\overline{Nu}$		
	$Gr = 1$	$Gr = 10$	$Gr = 20$
0.2	2.180	3.019	3.351
0.5	1.603	2.272	2.545
0.8	1.158	1.699	1.923

η. This re-inforces the finding cited in [29,30], namely that the heat transfer rate is enhanced as the ellipse gets thinner

Table 4
Average Nusselt numbers for various Grashof numbers and Prandtl numbers with $r = 0.5$ and $\eta = 45°$

Pr	$\overline{Nu}$		
	$Gr = 1$	$Gr = 10$	$Gr = 20$
0.7	1.484	2.103	2.343
1	1.603	2.272	2.545
5	2.223	3.331	3.743
10	2.580	3.892	4.481

and points to an important application for using elliptic tubes over circular tubes. Lastly, $\overline{Nu}$ increases slowly as η increases from 0° to 90°. Additional isotherm plots are displayed in Figs. 5 and 6 with Fig. 5 illustrating a symmetrical case having $\eta = 0$. Figs. 6a–6d, on the other hand, illustrate the changes in the isotherm plots as a result of varying Gr, Pr and r. To bring out these differences each diagram uses the same plotting parameters. The effect of increasing Gr is clearing seen by comparing Figs. 6a and 6b. As Gr is increased the thermal plume becomes narrower. The effect of increasing Pr is seen by comparing Figs. 6a and 6c and also results in a narrower plume, as expected. Lastly, the effect of varying the ellipse aspect ratio r is portrayed in Figs. 6b and 6d. It is interesting to observe that the thinner cylinder causes an enhanced rotation of the plume with the vertical.

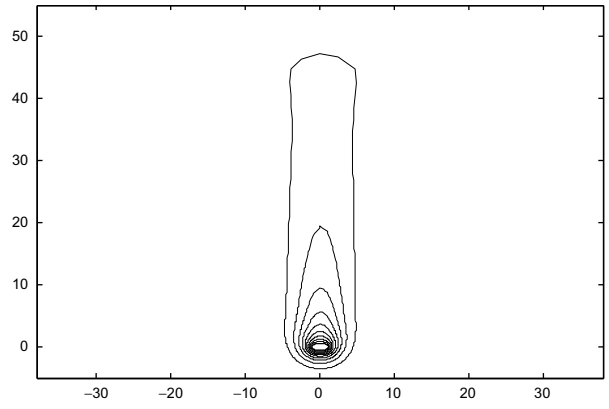

Fig. 5. Steady isotherm plot for the case $Gr = 1, Pr = 1, r = 0.5, \eta = 0°$.

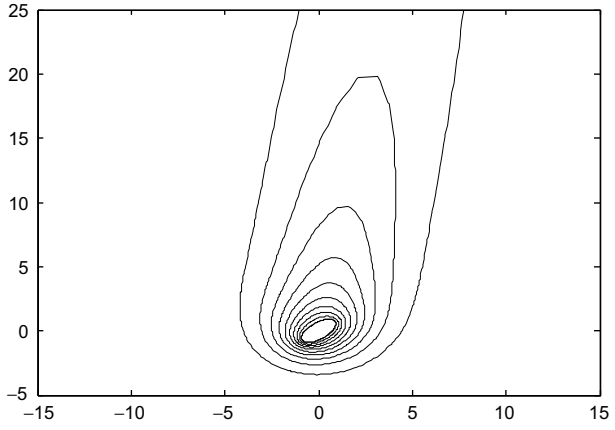

Fig. 6a. Steady isotherm plot for the case $Gr = 1, Pr = 1, r = 0.5, \eta = 45°$.

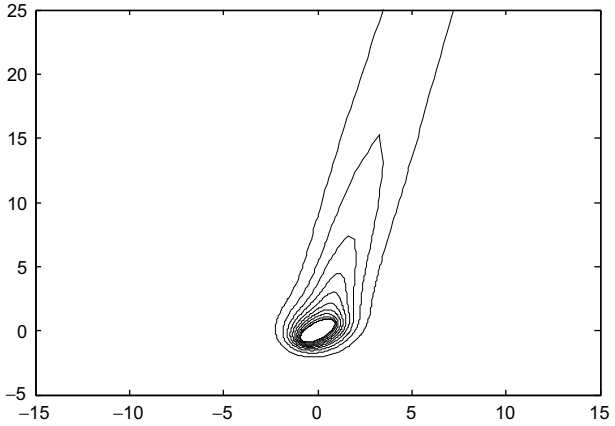

Fig. 6b. Steady isotherm plot for the case $Gr = 20, Pr = 1, r = 0.5, \eta = 45°$.

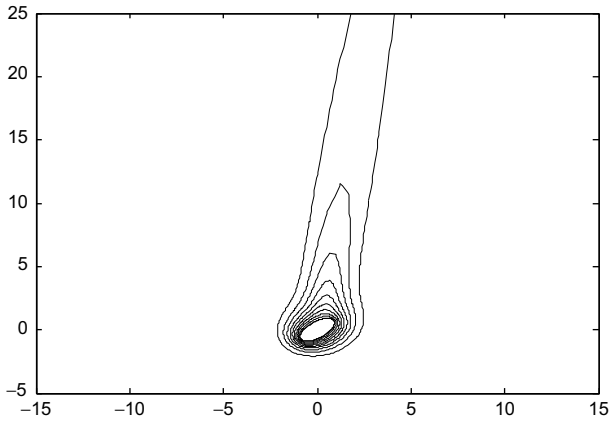

Fig. 6c. Steady isotherm plot for the case $Gr = 1, Pr = 10, r = 0.5, \eta = 45°$.

4.2. Unsteady results

In solving the unsteady problem, Eqs. (7)–(9) were integrated in the boundary-layer coordinate z up to a time $t = 0.25$ and then Eqs. (1), (4), and (5) were solved in the physical coordinate ξ. The approximate solution presented in Appendix B was used as an initial condition at $t = 0.01$. Suitable computational parameters for solving (7)–(9) were found to be $z_\infty = 5$, $N \times L = 101 \times 121$ and the number of terms retained in the Fourier series for computing the surface vorticity was $K = 25$. Initially, small time steps of $\Delta t = 10^{-3}$ were taken for the first 10 advances. Following that, time steps of $\Delta t = 10^{-2}$ were used up to $t = 0.25$. In the physical coordinate integration was continued with $\Delta t = 0.05$. With the passage of time the flow occupied more space, and thus, the outer boundary ξ_∞ had to be placed further away from the cylinder. This meant expanding the grid in order to capture the entire flow. For example, with $Gr = 1$, $\xi_\infty = 5$ was sufficient up until $t \sim 5$. The grid

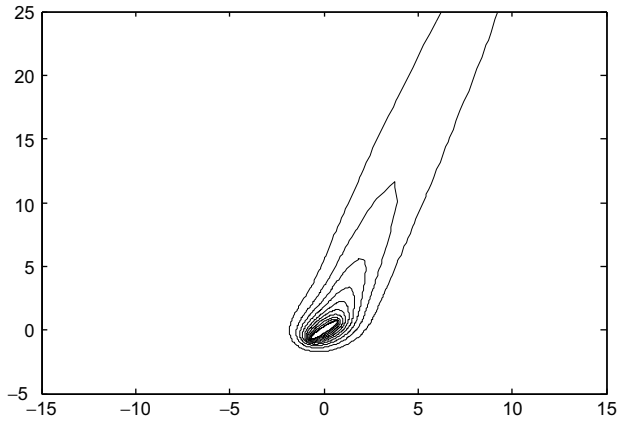

Fig. 6d. Steady isotherm plot for the case $Gr = 20, Pr = 1, r = 0.2, \eta = 45°$.

was then expanded to $N \times L = 201 \times 121$ (i.e., $\xi_\infty = 10$) which was satisfactory for times up to $t \sim 30$. Clearly, the longer the computations were carried out the further away ξ_∞ had to be placed. The convergence criterion employed for solving the unsteady problem was similar to that applied to the steady-state problem. As in the steady-state case, under-relaxation was applied to the surface vorticity. For this choice of computational parameters no convergence problems were encountered.

Table 5
Comparison of steady-state values of $\overline{Nu}$ with unsteady limits for $Gr = 1, 10$ for the case with $Pr = 1$, $\eta = 45°$ and $r = 0.5$

Gr	Steady-state $\overline{Nu}$	Unsteady limit $\overline{Nu}$
1	1.603	1.518
10	2.272	2.164

The main objective for performing the unsteady calculations was to investigate whether the long-time unsteady results converged to the corresponding steady results. Fig. 7 compares the steady and limiting ($t = 30$) unsteady Nusselt number distributions and reveals good agreement between the two. Fig. 8 illustrates the time variation of the average Nusselt number ($\overline{Nu}$) for $Gr = 1, 10$ while Table 5 compares numerical values. The time variations of $\overline{Nu}$ display convergence in $\overline{Nu}$ to a constant value. Note that at $t = 0$ the average Nusselt number is infinite due to

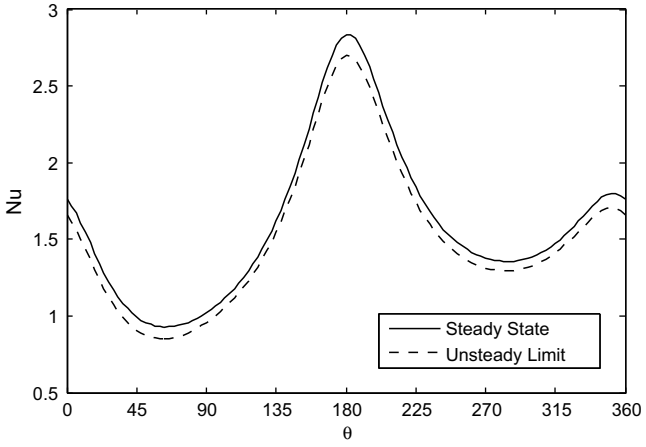

Fig. 7. Comparison of steady-state Nu distribution with unsteady limit for the case $Gr = 1, Pr = 1, r = 0.5, \eta = 45°$.

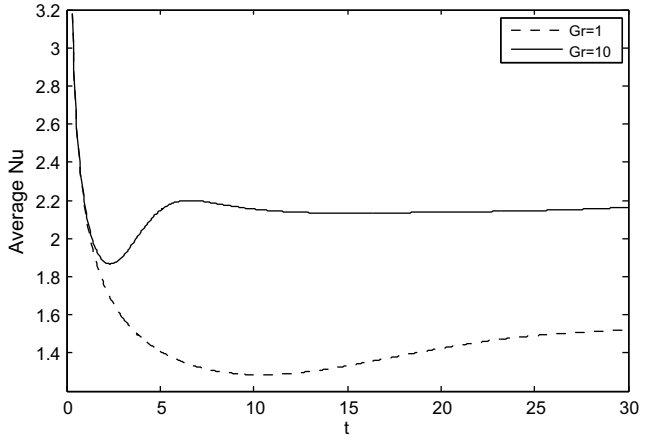

Fig. 8. Time variation of $\overline{Nu}$ for $Gr = 1, 10$ with $Pr = 1, r = 0.5, \eta = 45°$.

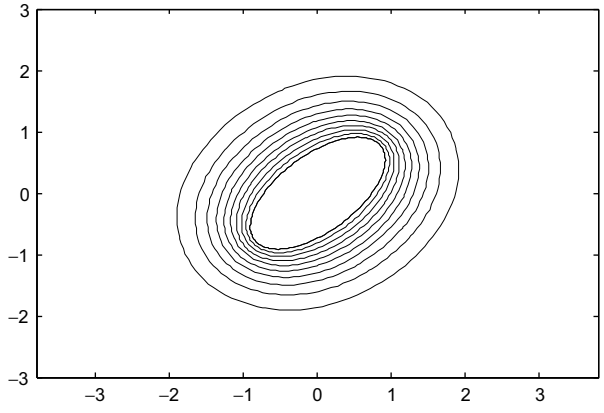

Fig. 9a. Unsteady isotherm plot at $t = 0.25$ for the case $Gr = 1, Pr = 1, r = 0.5, \eta = 45°$.

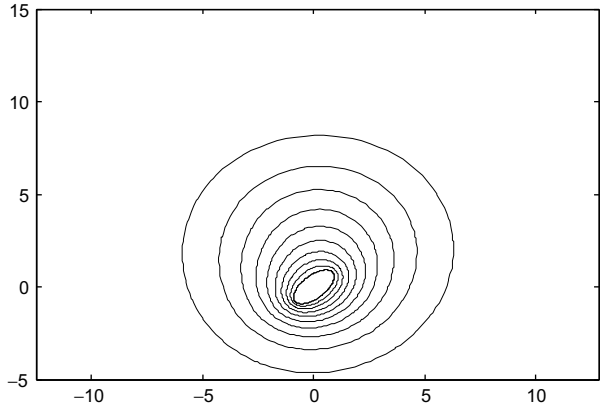

Fig. 9b. Unsteady isotherm plot at $t = 10$ for the case $Gr = 1$, $Pr = 1, r = 0.5, \eta = 45°$.

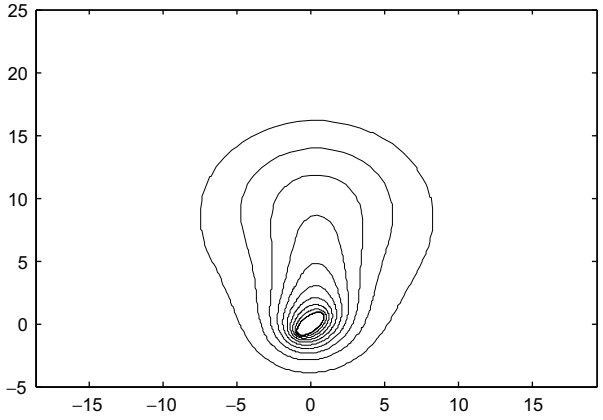

Fig. 9c. Unsteady isotherm plot at $t = 20$ for the case $Gr = 1, Pr = 1$, $r = 0.5, \eta = 45°$.

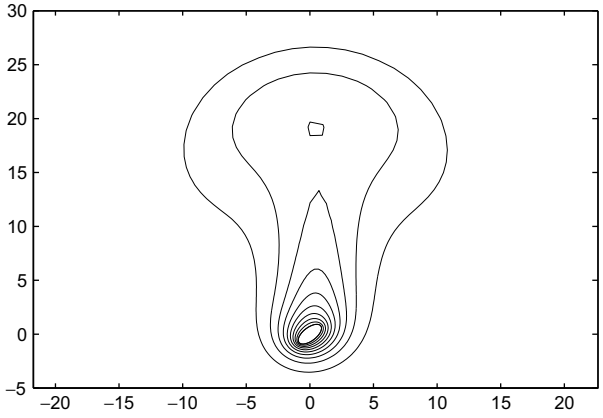

Fig. 9d. Unsteady isotherm plot at $t = 29.5$ for the case $Gr = 1, Pr = 1$, $r = 0.5, \eta = 45°$.

the temperature discontinuity on the cylinder surface and decays rapidly for $0 < t < 1$. Figs. 7 and 8 together with Table 5 suggest that near the cylinder surface the limiting unsteady solution approaches the steady-state solution, at least for the small Gr range.

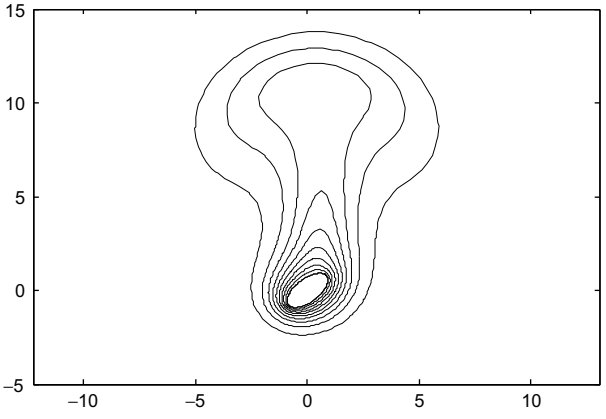

Fig. 10a. Unsteady isotherm plot at $t = 6$ for the case $Gr = 10, Pr = 1$, $r = 0.5, \eta = 45°$.

The situation further away from the cylinder is interestingly different though. Portrayed in Figs. 9a–9d are isotherm plots at various times for the case $Gr = 1, Pr = 1$,

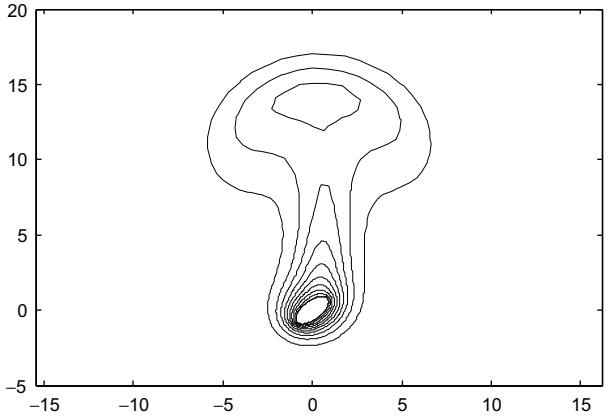

Fig. 10b. Unsteady isotherm plot at $t = 7$ for the case $Gr = 10, Pr = 1$, $r = 0.5, \eta = 45°$.

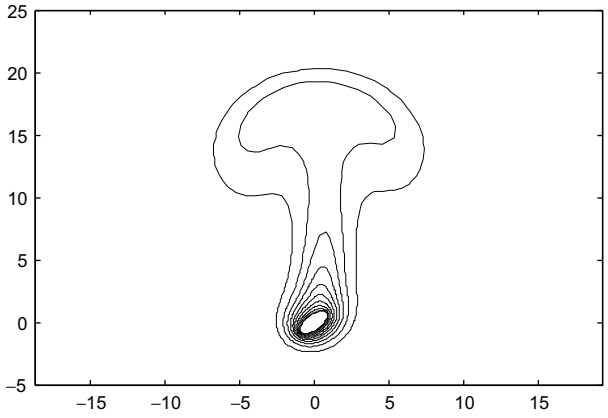

Fig. 10c. Unsteady isotherm plot at $t = 8$ for the case $Gr = 10, Pr = 1$, $r = 0.5, \eta = 45°$.

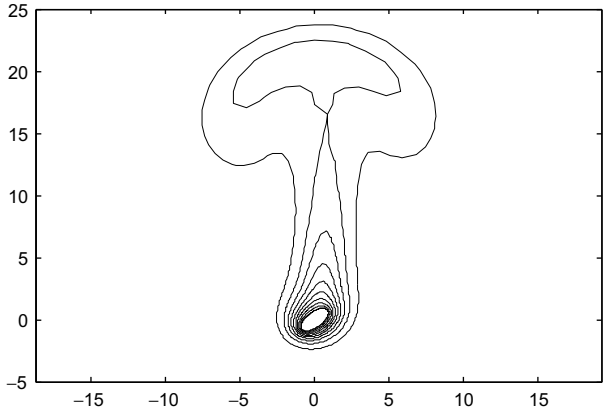

Fig. 10d. Unsteady isotherm plot at $t = 9$ for the case $Gr = 10, Pr = 1$, $r = 0.5, \eta = 45°$.

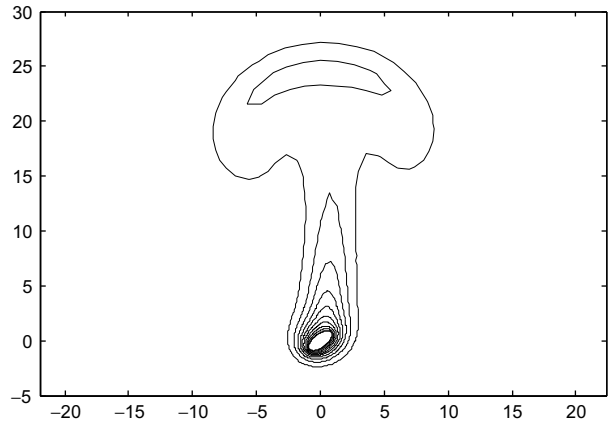

Fig. 10e. Unsteady isotherm plot at $t = 10$ for the case $Gr = 10, Pr = 1$, $r = 0.5, \eta = 45°$.

$r = 0.5$ and $\eta = 45°$. For small times, as seen in Fig. 9a, the isotherms appear to form concentric rings. This is to be expected since for small times the dominant heat transfer mechanism is conduction. As time evolves, depicted in Figs. 9b–9d, a well developed thermal plume forms. At $t = 29.5$ shown in Fig. 9d we notice the formation of a bubble which is clearly not consistent with the corresponding steady-state case shown in Fig. 6a. This inconsistency is even more evident when the Grashof number is increased to $Gr = 10$ as illustrated in Figs. 10a–10e. Thus, the unsteady far-field flow does not appear to approach a steady pattern. Instead, bubbles erupt periodically, probably as a result of an instability, and are swept to infinity.

5. Conclusions

Discussed and contrasted in this paper are two aspects related to free convection from an inclined elliptic cylinder. These include the steady-state (or time-independent) case and the unsteady (or time-dependent) case. The underlying assumptions made in this study include two-dimensionality of the flow, the validity of the Boussinesq approximation, the neglect of viscous dissipation, and that the flow remains laminar. This problem was investigated for the small Grashof number regime both numerically and analytically. The steady calculations support the finding that the rate of heat transfer is increased as the ellipse gets thinner.

While there was good agreement between the computed steady and limiting unsteady surface vorticity and Nusselt number distributions, noticeable differences were observed in the far-field isotherm plots. The unsteady problem reveals that the flow at large distances does not approach the static situation demonstrated by the steady-state problem. Instead, the outer isotherms form kinks which ultimately detach to form bubbles. This is presumably the result of an instability originating in the far-field. Due to buoyancy these bubbles continue to rise and float to infinity. Bubble formation becomes more and more vigorous as the Grashof number is increased.

Acknowledgements

Financial support for this research was provided by the Natural Sciences and Engineering Research Council of Canada. Discussions with Francis Poulin of UW are gratefully acknowledged.

Appendix A. Asymptotic solution

In solving the steady-state problem the far-field conditions $\psi, \zeta, \phi \to 0$ as $\xi \to \infty$ are imposed. Computationally, the outer boundary ξ_∞ is used to approximate infinity. As a compromise between computational efficiency and mathematical correctness it is desirable to derive more appropriate conditions that can be applied along the boundary ξ_∞. One approach in obtaining these far-field conditions is to make use of the well-known similarity solution from a line heat source, since at large distances the cylinder will appear as a line. While this approach seems promising there are some serious drawbacks. For example, the similarity solution is based on the boundary-layer equations and for small Grashof numbers as considered here, these equations do not apply. Further, as pointed out by Suriano and Yang [2], the vertical velocity predicted by the similarity solution increases without bound with distance from the source and this behaviour is clearly not physical. For these reasons a different approach was adopted.

We begin by arguing that at large distances the flow will eventually become symmetrical and the cylinder can be viewed as circular. Then, the working equations become

$$\frac{\partial^2\psi}{\partial\xi^2} + \frac{\partial^2\psi}{\partial\theta^2} = e^{2\xi}\zeta, \tag{A1}$$

$$\frac{\partial^2\zeta}{\partial\xi^2} + \frac{\partial^2\zeta}{\partial\theta^2} = \frac{\partial\psi}{\partial\xi}\frac{\partial\zeta}{\partial\theta} - \frac{\partial\psi}{\partial\theta}\frac{\partial\zeta}{\partial\xi} + Gre^{\xi}\left(\sin\theta\frac{\partial\phi}{\partial\xi} + \cos\theta\frac{\partial\phi}{\partial\theta}\right), \tag{A2}$$

$$\frac{\partial^2\phi}{\partial\xi^2} + \frac{\partial^2\phi}{\partial\theta^2} = Pr\left(\frac{\partial\psi}{\partial\xi}\frac{\partial\phi}{\partial\theta} - \frac{\partial\psi}{\partial\theta}\frac{\partial\phi}{\partial\xi}\right). \tag{A3}$$

Here, the conformal mapping is given by $x + iy = e^{\xi+i\theta}$. In addition, the geometry has been configured so that the x-axis points in the vertical direction so as to be consistent with common convention used in previous investigations and also for convenience in imposing symmetry.

Next, we set $\psi = \psi^* + \hat{\psi}$ where ψ^* represents the correction to the irrotational solution, $\hat{\psi}$, which is obtained by solving

$$\frac{\partial^2\hat{\psi}}{\partial\xi^2} + \frac{\partial^2\hat{\psi}}{\partial\theta^2} = 0. \tag{A4}$$

The symmetrical solution to (A4) satisifying $\hat{\psi} \to 0$ as $\xi \to \infty$ is given by

$$\hat{\psi}(\xi,\theta) = \sum_{n=1}^{\infty} a_n e^{-n\xi}\sin(n\theta).$$

Retaining the leading-order term, which we assume corresponds to $n = 1$, we then set

$$\psi = \psi^* + a_1 e^{-\xi} \sin\theta,$$

where a_1 is an arbitrary constant. Using this formulation the linearized heat equation, which will be valid at large distances, then becomes

$$\frac{\partial^2\phi}{\partial\xi^2} + \frac{\partial^2\phi}{\partial\theta^2} + a_1 Pr e^{-\xi}\left(\cos\theta\frac{\partial\phi}{\partial\xi} + \sin\theta\frac{\partial\phi}{\partial\theta}\right) = 0. \tag{A5}$$

To solve Eq. (A5) we introduce $\chi = e^{-a_1 Pr e^{-\xi}\cos\theta/2}\phi$ which satisfies

$$\frac{\partial^2\chi}{\partial\xi^2} + \frac{\partial^2\chi}{\partial\theta^2} - \frac{a_1^2 Pr^2}{4} e^{-2\xi}\chi = 0. \tag{A6}$$

The solution obeying $\chi \to 0$ as $\xi \to \infty$ is

$$\chi(\xi,\theta) = \sum_{n=1}^{\infty}[b_n \sin(n\theta) + c_n \cos(n\theta)] I_n(a_1 Pr e^{-\xi}/2),$$

where I_n denotes the modified Bessel function of order n of the first kind. For large ξ, I_n is well approximated by the leading-order term in its asymptotic expansion given by

$$I_n \sim \frac{a_1^n Pr^n}{2^{2n} n!} e^{-n\xi} \quad \text{as} \quad \xi \to \infty.$$

Taking the symmetrical solution of order m to be the first non-zero term in the series yields the following asymptotic solution for ϕ:

$$\phi \sim e^{a_1 Pr e^{-\xi}\cos\theta/2}\{a_2 e^{-m\xi}\cos(m\theta)\},$$

where a_2 is an unknown constant. We point out that determining the order m is part of the solution procedure.

To an excellent approximation, the factor

$$e^{a_1 Pr e^{-\xi}\cos\theta/2} \approx 1 \quad \text{as} \quad \xi \to \infty.$$

However, it is worth emphasizing the importance of this factor. It accounts for the variation of ϕ in the plume region concentrated around $\theta = 0$. As expected, ϕ will decay more slowly in this region. For moderately large ξ we see that this variation is not significant. This marks a fundamental difference in the form of the solution when compared to the classical line source solution which emerges from the boundary-layer equations. It is also worth mentioning that when a background flow is present, such as in mixed convection problems, the above factor will display a more well defined plume region.

Next, we proceed to the vorticity equation. At large distances it is expected that a balance between diffusion and buoyancy will be reached and retaining the dominant terms in the vorticity equation gives

$$\frac{\partial^2\zeta}{\partial\xi^2} + \frac{\partial^2\zeta}{\partial\theta^2} = -m a_2 Gr e^{-(m-1)\xi}\sin[(m+1)\theta]. \tag{A7}$$

The solution to (A7) satisfying $\zeta \to 0$ as $\xi \to \infty$ is easily found to be

$$\zeta = \left(d_1 e^{-(m+1)\xi} + \frac{a_2 Gr}{4} e^{-(m-1)\xi}\right)\sin[(m+1)\theta],$$

where d_1 is an arbitrary constant.

Lastly, we return to the streamfunction and solve for ψ^* using the above result for the vorticity. This brings us to the equation

$$\frac{\partial^2\psi^*}{\partial\xi^2} + \frac{\partial^2\psi^*}{\partial\theta^2} = (d_1 e^{-(m-1)\xi} + \frac{a_2 Gr}{4} e^{-(m-3)\xi})\sin[(m+1)\theta]. \tag{A8}$$

It is immediately clear from (A8) that in order for $\psi^* \to 0$ as $\xi \to \infty$ we require that $m > 3$. Thus, setting $m = 4$ as the leading-order term we arrive at the following solution for ψ^*:

$$\psi^* = \left(-\frac{d_1}{16} e^{-3\xi} + d_2 e^{-5\xi} - \frac{a_2 Gr}{96} e^{-\xi}\right)\sin(5\theta),$$

where d_2 is another arbitrary constant. It is interesting to observe that the dominant term in this solution is $O(e^{-\xi})$ just like the irrotational solution. Thus, the rotational component of the vorticity contributes little in the far-field. Summarizing, we have found that

$$\psi \sim a_1 e^{-\xi}\sin\theta, \quad \zeta \sim \frac{a_2 Gr}{4} e^{-3\xi}\sin(5\theta),$$
$$\phi \sim a_2 e^{-4\xi}\cos(4\theta) \quad \text{as} \quad \xi \to \infty.$$

From the above, it is clear that neglecting the advective term in the vorticity equation is justified since it is $O(e^{-4\xi})$ while the buoyancy term is $O(e^{-3\xi})$.

To deal with the unknown constants a_1 and a_2, several approaches can be taken. Ideally, they should be related to macroscopic quantities such as the drag/ lift coefficients and $\overline{Nu}$, although this may be complicated to do. Another approach would be to determine them numerically by appealing to the integral conditions discussed earlier. By splitting the integrals into two parts, one from $0 \leqslant \xi \leqslant \xi_\infty$ and the other from $\xi_\infty \leqslant \xi < \infty$, we can compute the first part numerically and the second part analytically using the asymptotic solution. The constants can then be determined numerically as part of the iterative procedure. Alternatively, the above asymptotic conditions can be converted to the following gradient conditions:

$$\frac{\partial\psi}{\partial\xi} \to -\psi, \quad \frac{\partial\zeta}{\partial\xi} \to -3\zeta, \quad \frac{\partial\phi}{\partial\xi} \to -4\phi \quad \text{as} \quad \xi \to \infty,$$

which do not involve the unknown constants. These conditions are consistent with the asymptotic solutions and are more convenient to implement in a numerical solution procedure.

Appendix B. Derivation of small time solution

The leading-order terms ψ_*, ζ_*, ϕ_* are expected to be dictated by the conduction equations

$$\frac{\partial^2\psi_*}{\partial\xi^2} = M_0^2\zeta_*,$$
$$\frac{\partial\zeta_*}{\partial t} = \frac{1}{M_0^2}\left[\frac{\partial^2\zeta_*}{\partial\xi^2} + GrA_0\frac{\partial\phi_*}{\partial\xi}\right],$$
$$\frac{\partial\phi_*}{\partial t} = \frac{1}{M_0^2 Pr}\frac{\partial^2\phi_*}{\partial\xi^2},$$

where

$$M_0^2(\theta) = \frac{1}{2}[\cosh(2\xi_0) - \cos(2\theta)],$$
$$A_0(\theta) = \sinh\xi_0\cos\eta\cos\theta - \cosh\xi_0\sin\eta\sin\theta.$$

Similarity solutions for ϕ_*, ζ_* with $Pr = 1$ satisfying the boundary conditions are found to be

$$\phi_* = \mathrm{erfc}(M_0 z),$$
$$\zeta_* = \frac{\sqrt{t}}{2}\left[\frac{1}{\sqrt{\pi}M_0}\mathrm{e}^{-M_0^2z^2} - z\,\mathrm{erfc}(M_0 z)\right]H(\theta) + GrA_0\sqrt{t}\left[\frac{1}{\sqrt{\pi}M_0}\mathrm{e}^{-M_0^2z^2} - 2z\,\mathrm{erfc}(M_0 z)\right],$$

where

$$\mathrm{erfc}(x) = 1 - \frac{2}{\sqrt{\pi}}\int_0^x \mathrm{e}^{-u^2}\mathrm{d}u, \quad z = \frac{\xi}{\sqrt{4t}},$$

and $H(\theta)$ is an arbitrary function.

The similarity solution suggests that we consider rescaling the coordinate ξ as $\xi = \sqrt{4t}z$. The transformed equations are given by Eqs. (7)–(9). The similarity solution also suggests that for small t we can expand the flow variables in the following series:

$$\psi = \psi_0 + \sqrt{t}\psi_1 + t\psi_2 + \cdots,$$
$$\zeta = \zeta_0 + \sqrt{t}\zeta_1 + t\zeta_2 + \cdots,$$
$$\phi = \phi_0 + \sqrt{t}\phi_1 + t\phi_2 + \cdots$$

It follows that the similarity solutions will emerge naturally from this expansion procedure. To proceed we next expand quantities such as $\mathrm{e}^{-2n\sqrt{t}z}, A, B$ and M^2 in the series

$$\mathrm{e}^{-2n\sqrt{t}z} = 1 - 2n\sqrt{t}z + 2n^2tz^2 - \cdots,$$
$$A(z,\theta,t) = A_0(\theta) + 2\sqrt{t}zA_1(\theta) + 2tz^2A_0(\theta) + \cdots,$$
$$B(z,\theta,t) = B_0(\theta) + 2\sqrt{t}zB_1(\theta) + 2tz^2B_0(\theta) + \cdots,$$
$$M^2(z,\theta,t) = M_0^2(\theta) + 2\sinh(2\xi_0)\sqrt{t}z + 4\cosh(2\xi_0)tz^2 + \cdots,$$

where

$$A_1(\theta) = \cosh\xi_0\cos\eta\cos\theta - \sinh\xi_0\sin\eta\sin\theta,$$
$$B_0(\theta) = \cosh\xi_0\cos\eta\sin\theta + \sinh\xi_0\sin\eta\cos\theta,$$
$$B_1(\theta) = \sinh\xi_0\cos\eta\sin\theta + \cosh\xi_0\sin\eta\cos\theta.$$

Substituting these expansions into Eqs. (7)–(9) and equating like powers of t leads to a hierarchy of problems at various levels of approximation. We have explicitly determined the non-zero terms ζ_1, ϕ_0, ϕ_1 and have deduced that $\psi_0 = \psi_1 = \psi_2 = \zeta_0 = 0$.

We illustrate the procedure for the $\mathrm{O}(\sqrt{t})$ problem. The terms ψ_1, ζ_1, ϕ_1 satisfy the equations

$$\frac{\partial^2\psi_1}{\partial z^2} = 0,$$
$$\frac{1}{M_0^2}\frac{\partial^2\zeta_1}{\partial z^2} + 2z\frac{\partial\zeta_1}{\partial z} - 2\zeta_1 = -\frac{2GrA_0}{M_0^2}\frac{\partial\phi_0}{\partial z},$$
$$\frac{1}{PrM_0^2}\frac{\partial^2\phi_1}{\partial z^2} + 2z\frac{\partial\phi_1}{\partial z} - 2\phi_1 = -\frac{4\sinh(2\xi_0)z^2}{M_0^2}\frac{\partial\phi_0}{\partial z},$$

where

$$\phi_0(z,\theta) = \mathrm{erfc}(\sqrt{Pr}M_0 z).$$

The solution for ψ_1 satisfying $\psi_1 = \partial\psi_1/\partial z = 0$ on $z = 0$ is easily found to be $\psi_1(z,\theta) = 0$. By variation of parameters the solution for ϕ_1 satisfying $\phi_1 = 0$ on $z = 0$ and $\phi_1 \to 0$ as $z \to \infty$ is given by

$$\phi_1(z,\theta) = -\frac{\sinh(2\xi_0)z}{\sqrt{\pi}M_0^2}\left[\sqrt{Pr}M_0 z\mathrm{e}^{-PrM_0^2z^2} + \frac{\sqrt{\pi}}{2}\mathrm{erfc}(\sqrt{Pr}M_0 z)\right].$$

To solve for ζ_1 we set $Pr = 1$ so as to simplify the algebra, and impose the boundary condition $\zeta_1 \to 0$ as $z \to \infty$. Since the surface vorticity is not known, we also enforce the integral conditions which have been expanded to yield

$$\int_0^\infty\int_0^{2\pi} M_0^2\zeta_1\sin(n\theta)\mathrm{d}\theta\mathrm{d}z = 0, \quad n = 1,2,\ldots,$$
$$\int_0^\infty\int_0^{2\pi} M_0^2\zeta_1\cos(n\theta)\mathrm{d}\theta\mathrm{d}z = 0, \quad n = 0,1,\ldots$$

The general solution for ζ_1 is

$$\zeta_1(z,\theta) = C(\theta)M_0 z + D(\theta)[\mathrm{e}^{-M_0^2z^2} + \sqrt{\pi}M_0 z\,\mathrm{erf}(M_0 z)] - \frac{GrA_0}{\sqrt{\pi}M_0}\mathrm{e}^{-M_0^2z^2}.$$

Since $\zeta_1 \to 0$ as $z \to \infty$, it follows that $C(\theta) = -\sqrt{\pi}D(\theta)$. From the integral conditions we can deduce that

$$D(\theta) = \frac{2GrA_0}{\sqrt{\pi}M_0}.$$

Thus, the solution for ζ_1 becomes

$$\zeta_1(z,\theta) = \frac{GrA_0}{\sqrt{\pi}M_0}\mathrm{e}^{-M_0^2z^2} - 2GrA_0 z\,\mathrm{erfc}(M_0 z).$$

These non-zero terms are sufficient to yield an accurate solution for small t and can be used to furnish an initial condition for small times beyond $t = 0$. This expansion procedure can be continued. More terms have been found and are reported in [31]. Since the analytical solutions presented here have only been found for $Pr = 1$, the more general case with $Pr \neq 1$ can be found by numerically solving the corresponding equations.

References

[1] A.P. Bassom, P.J. Blennerhassett, Impulsively generated convection in a semi-infinite fluid layer above a heated flat plate, Q.J. Mech. Appl. Math. 55 (2002) 573–595.

[2] F.J. Suriano, K.T. Yang, Laminar free convection about vertical and horizontal plates at small and moderate Grashof numbers, Int. J. Heat Mass Transfer 11 (1968) 473–492.
[3] S.W. Churchill, H.H. Chu, Correlating equations for laminar and turbulent free convection from a vertical plate, Int. J. Heat Mass Transfer 18 (1975) 1323–1329.
[4] R.J. Goldstein, D.G. Briggs, Transient free convection about vertical plates and circular cylinders, ASME J. Heat Transfer 86C (1964) 490–500.
[5] N.E. Hardwick, E.K. Levy, Study of laminar free convection wake above an isothermal vertical plate, ASME J. Heat Transfer 95 (1973) 289–294.
[6] E.M. Sparrow, S.V. Patanker, R.M. Abdel-Wahed, Development of wall and free plumes above a heated vertical plate, ASME J. Heat Transfer 100 (1978) 184–190.
[7] R. Chouikh, A. Guizani, M. Maalej, A. Gelghith, Numerical study of the laminar natural convection flow around horizontal isothermal cylinder, Renew. Energ. 13 (1998) 77–88.
[8] T. Saitoh, T. Sajiki, K. Maruhara, Bench mark solutions to natural convection heat transfer problem around a horizontal circular cylinder, Int. J. Heat Mass Transfer 36 (1993) 1251–1259.
[9] M.A. Atmane, V.S.S. Chan, D.B. Murray, Natural convection around a horizontal heated cylinder: the effects of vertical confinement, Int. J. Heat Mass Transfer 46 (2003) 3661–3672.
[10] H.M. Badr, Heat transfer in transient buoyancy driven flow adjacent to a horizontal rod, Int. J. Heat Mass Transfer 30 (1987) 1997–2012.
[11] L. Elliot, Free convection on a two-dimensional or axisymmetric body, Q.J. Mech. Appl. Math. 23 (1970) 153–162.
[12] B. Farouck, S.I. Guceri, Natural convection from a horizontal cylinder – laminar regime, ASME J. Heat Transfer 103 (1981) 522–527.
[13] T.H. Kuehn, R.J. Goldstein, Numerical solution to the Navier–Stokes equations for laminar natural convection about a horizontal isothermal circular cylinder, Int. J. Heat Mass Transfer 23 (1980) 971–979.
[14] J.H. Merkin, Free convection on an isothermal horizontal cylinder, ASME paper No. 76-HT-16, 1976.
[15] L. Pera, B. Gebhart, Experimental observations of wake formation over cylindrical surfaces in natural convection flows, Int. J. Heat Mass Transfer 15 (1972) 175–177.
[16] H.M. Badr, K. Shamsher, Free convection from an elliptic cylinder with major axis vertical, Int. J. Heat Mass Transfer 36 (1993) 3593–3602.
[17] F.M. Mahfouz, S. Kocabiyik, Transient numerical simulation of buoyancy driven flow adjacent to an elliptic tube, Int. J. Heat Fluid Flow 24 (2003) 864–873.
[18] H.M. Badr, Laminar natural convection from an elliptic tube with different orientations, J. Heat Transfer 119 (1997) 709–718.
[19] S.Y. Huang, F. Mayinger, Heat transfer with natural convection around elliptic tubes, Warme-Und Stoffubertragung 18 (1984) 175–183.
[20] A.O. Elsayed, E.Z. Ibrahim, S.A. Elsayed, Free convection from a constant heat flux elliptic tube, Energ. Convers. Manage. 44 (2003) 2445–2453.
[21] F.N. Lin, B.T. Chao, Laminar free convection over two-dimensional and axisymmetric bodies of arbitrary contour, ASME J. Heat Transfer 96 (1974) 435–442.
[22] J.H. Merkin, Free convection boundary layers on cylinders of elliptic cross section, ASME J. Heat Transfer 99 (1977) 453–457.
[23] G.D. Raithby, K.G. Hollands, Laminar and turbulent free convection from elliptic cylinders with a vertical plate and horizontal circular cylinder as special cases, ASME J. Heat Transfer 98 (1976) 72–80.
[24] T. Fujii, Theory of the steady laminar natural convection above a horizontal line heat source and a point heat source, Int. J. Heat Mass Transfer 6 (1963) 597–606.
[25] T. Fujii, I. Morioka, H. Uehara, Buoyant plume above a horizontal line heat source, Int. J. Heat Mass Transfer 16 (1973) 755–768.
[26] S.C.R. Dennis, L. Quartapelle, Some uses of Green's theorem in solving the Navier–Stokes equations, Int. J. Numer. Meth. Fluids 9 (1989) 871–890.
[27] S.J.D. D'Alessio, M.G. Saunders, D.L. Harmsworth, Mixed convective heat transfer from an accelerating elliptic cylinder, Int. J. Heat Mass Transfer 46 (2003) 2927–2946.
[28] S.C.R. Dennis, J.D. Hudson, Compact h^4 finite-difference approximations to operators of Navier–Stokes type, J. Comp. Phys. 85 (1989) 390–416.
[29] G.P. Fieg, W. Roetzel, Calculation of laminar film condensation in/on inclined elliptical tubes, Int. J. Heat Mass Transfer 37 (1994) 619–624.
[30] S.B. Memory, V.H. Adams, P.J. Marto, Free and forced convection laminar film condensation on horizontal elliptical tubes, Int. J. Heat Mass Transfer 40 (1997) 3395–3406.
[31] M.L. Williams, Analytic study of unsteady free convection from an inclined elliptic cylinder, M. Math. thesis, University of Waterloo, Waterloo, Ontario, 2004.